Vol. 19, n.° 3, pp. 117-130, 2020

Revista UIS Ingenierías

Página de la revista: revistas.uis.edu.co/index.php/revistauisingenierias

Non-linear controller for storage systems with regulated output voltage and safe current slew-rate for the battery

Controlador no-lineal para sistemas de almacenamiento con voltaje de salida regulado y derivada de corriente segura para la batería

Carlos Andrés Ramos-Paja [1], Juan David Bastidas-Rodríguez [2], Daniel González-Montoya [3]

[1] Facultad de Minas, Universidad Nacional de Colombia, Medellín, Colombia. Orcid: 0000-0003-2231-4177. Email: caramosp@unal.edu.co

[2] Facultad de Ingeniería y Arquitectura, Universidad Nacional de Colombia, Manizales, Colombia. Orcid: 0000-0002-4634-2642. Email: jubastidasr@unal.edu.co

[3] Departamento de Electrónica y Telecomunicaciones, Instituto Tecnológico Metropolitano, Medellín, Colombia. Email: danielgonzalez@itm.edu.co

Received: 15 January 2020. Accepted: 15 March 2020. Final version: 25 May 2020

Abstract

This paper proposes a non-linear control structure for a hybrid energy storage system with a series architecture, which regulates the voltage of a DC bus (output voltage) and ensures that the battery current fulfills the current slew-rate restriction. The proposed solution has two stages, in the first one, the battery is connected to a buck/boost converter that feeds an auxiliary capacitor. In the second stage, the auxiliary capacitor is connected to a DC bus through a second buck/boost converter. Both converters are regulated using cascaded control systems, where the inner loops are slidingmode controllers of the inductors' current, and the outer loops in the first and second converter are designed to limit the slew-rate of the battery current and to regulate the dc bus voltage, respectively. The paper provides the design procedure for the controllers and validates its performance with simulation results for the power system operating in charging, discharging and stand-by modes.

Keywords: battery; capacitor; buck/boost converter; current slew-rate; sliding-mode control.

Resumen

Este artículo propone una estructura de control no-lineal para un sistema de almacenamiento híbrido con una arquitectura en serie, en la cual se regula la tensión de un bus DC (voltaje de salida) y asegura que la corriente de la batería cumpla con la restricción de velocidad de cambio en la corriente. La solución propuesta tiene dos etapas, en la primera se conecta una batería a un convertidor buck/boost que alimenta un capacitor auxiliar. En la segunda etapa, el capacitor auxiliar se conecta a un bus de DC a través de un segundo convertidor buck/boost. Ambos convertidores se regulan utilizando sistemas de control en cascada, donde los lazos internos son controladores por modos deslizantes de las corrientes de los inductores, y los lazos externos del primer y el segundo convertidor se diseñan para limitar la velocidad de cambio de la corriente en la batería y regular la tensión en el bus de DC, respectivamente. El artículo proporciona el procedimiento de diseño para los controladores y valida su desempeño con resultados de simulación considerando el sistema de potencia operando en modos de carga, descarga y almacenamiento.

ISSN impreso: 1657 - 4583. ISSN en línea: 2145 – 8456,

C. Ramos, J. Bastidas, D. González, "Non-linear controller for storage systems with regulated output voltage and safe current slew-rate for the battery," *Rev. UIS Ing.*, vol. 19, no. 3, pp. 117-130, 2020. doi: https://doi.org/10.18273/revuin.v19n3-2020012

Palabras clave: batería; capacitor; convertidor buck/boos; velocidad de cambio de la corriente; control por modos deslizantes.

1. Introduction

Nowadays, there are different applications that require an Energy Storage System (ESS) like microgrids, standalone renewable energy systems, electric transport systems, uninterruptible power supply, among others. Such a necessity of ESS have produce a continuous growth of the global installed storage capacity, which was estimated as 15.3 GWh in 2017, excluding pumped hydro [1]. From such a capacity it is important to highlight that lithium-ion batteries have been widely used in the last years to implement ESS, since in 2016 88 % of the deployed storage capacity correspond to this technology [1].

In many applications (e.g. microgrids, electric vehicles, stand-alone photovoltaic systems) batteries are used to regulate the voltage of a DC bus by compensating the differences between generation and load. Such a compensation is performed by charging/discharging the batteries when the load is greater/less than the generation. The power provided/extracted to the DC bus from the batteries is performed through a charging/discharging system that is formed by a power converter and a control system.

Usually the battery voltage is less than the DC bus voltage, therefore, bidirectional boost converters are used to implement the charging/discharging system [2]. Nevertheless, a battery or battery bank may have voltages equal or greater than the DC bus; therefore, step-up/down converters are a more flexible solution for charging discharging systems [3, 4]. Moreover, the current required from the battery to regulate the DC bus depends on the load profiles that disturb the DC bus voltage. Therefore, fast variations in the load may produce high current derivatives in the battery that surpass the slew-rate limitations defined by the manufacturers [5]. Those high current derivatives may significantly reduce the battery lifetime [5]; then, the current slew-rate limitation is an important part of a charging/discharging system.

One option to address this problem is to construct Hybrid Energy Storage Systems (HESSs) with batteries and supercapacitors (SCs), where the low frequency currents required by the load are provided by the battery and the high frequency currents (transients) are supplied by the SC [2]. In general, a HESS can be used in any application with load perturbations that demand high slew-rate currents from the batteries. However, in the literature the main applications of HESS are the DC bus voltage regulation in: microgrids [5, 6, 7, 8, 9, 10], electric vehicles [11, 12, 13, 14, 15, 16, 17, 18], systems with a generic load [19, 20], and systems with renewable energy sources like photovoltaic [21], wind turbines [22] and fuel cells [20].

In microgrids, the HESS compensates the differences between the unpredictable energy sources and loads to keep the microgrid stability; while in electric vehicles the HESS provide the variable power required by the motor and absorbs the energy from the regenerative brakes. Finally, in systems with unpredictable energy sources the HESS may compensate the excess/lack of power production by charging/discharging the HESS to supply energy required by the load.

In the literature there are different HESS architectures for the HESS, as shown in [2]; however, the parallel architecture is the most widely used. In this architecture, the battery and the SC are connected to the DC bus using two power converters with the outputs connected in parallel [5, 6, 7, 8, 10, 11, 12, 14, 18, 20, 21, 23]; therefore, the battery and the SC can be independently controlled to use the SC as a power source to compensate fast perturbations in the load and the battery to supply/absorb the long-term energy required/provided by the DC bus. HESS with series architecture are also reported in the literature, which use one converter to connect the SC to the DC bus and the battery is connected in parallel to the DC bus (i.e. without converter) [13, 19, 24] or vice-versa [15]. In those cases, the storage device without converter (SC or battery) cannot be controlled, hence, it is difficult to guarantee that the fast perturbations of the load are supplied by the SC to protect the battery. Moreover, in other papers the HESS topology is not clearly explained [22].

Regarding the power converters, most of the proposed HESS use boost [7, 8, 10, 11, 12, 15, 18, 21, 22, 23, 24] converters to connect the battery and the SC to the DC bus; while others use interleaved boost [13, 14], buck [19, 25], or a buck/boost operating as step-up converter [5, 6] to couple the SC and batteries to the DC bus. Therefore, most of the HESS the charging/discharging system work for battery and SC voltages less than the DC bus. Nonetheless, in some ESS technologies (like SC) the voltage significantly vary with the state-of-charge, as consequence its voltage may be less, greater or equal than the DC bus voltage. In those cases, some authors use step-up/down converters to increase the flexibility of the charging/discharging system [3, 4]. Additionally, it is worth noting that boost converters have the disadvantage of injecting discontinuous current to the DC bus; while

buck converters produce discontinuous currents in the storage devices.

Moreover, there are different control systems for HESS reported in the literature, some of them use linear controllers, while the others propose nonlinear controllers. The authors in [5, 6] propose cascade control structures with linear controllers, where the outer loop regulates the DC bus voltage in [6, 10, 13] and tracks a power reference in [5]; while the inner loops in [5, 6, 10, 13] track the current of the battery and SC with PI controllers.

Nevertheless, linear controllers cannot guarantee the system stability for all the operating conditions (i.e. no global stability), and their dynamic performance may vary depending on the operating point, since linear controllers are designed by using linearized models.

Some authors use nonlinear control systems based on Sliding-Mode Control (SMC) theory. On the one hand, in [11, 12, 24] the control system of the HESS is a multiple input multiple output SMC to regulate the DC bus voltage and control the current provided/absorbed by the battery and the SC. However, the design procedure of the control systems is not clearly explained and the DC bus voltage show significant oscillations where there are disturbances in the DC bus.

Moreover, the SMCs proposed in [11, 12] do not generate the switching signals of the power converters, since the SMCs are used to generate the PWM signals for the switches; as consequence, the system doesn't slide around a surface within a desired hysteresis band. On the other hand, in [21] the authors use two SMC controllers when the battery reaches its maximum and minimum currents (i.e. discharging and charging) and two passivity based multiple input multiple output controllers to regulate the DC bus voltage and the storage devices' currents. However, the design procedure is complex and the control system is formed by four controllers, which complicates its implementation.

The control systems proposed in [8, 20, 23] combine linear controllers and SMC in a cascade structure. The inner loops are SMC controllers of the battery and SC currents and the outer loops are PI regulators of the DC bus voltage. Nonetheless, the SMC controllers proposed in [8, 23] are used to generate the duty cycle of the power converters and not their switching signals. Additionally, the SMC proposed in [20] doesn't include the design procedure, nor the stability analysis.

Other authors propose HESS control systems based on adaptive SMCs for HESS in series architectures, where the SC [19] or the battery [15] are connected to the DC bus through power converters and the other storage device (i.e. battery in [19] and SC in [15]) is connected in parallel to the DC bus. The controller proposed in [19] modifies the sliding surface function depending if the SC current is between its maximum and minimum values, or if it reaches one of the limits. Although the authors provide the stability analysis and the design of the SMC parameters, the voltage of the SC is not controlled and the transition between one sliding surface to the other is not analyzed. The controller proposed in [15] uses a SMC for the battery current and a SMC-based observer for the battery voltage and the HESS output current to regulate the DC bus voltage. Nevertheless, the control only considers resistive loads and the SMC is used to calculate a duty cycle and not to generate the switching signals to slide around a surface.

Some approaches combine SMCs with other nonlinear controllers to construct the HESS control strategy. In [22] the authors use the desired output power of the HESS and a SMC theory to generate a surface and its derivative, which are used as inputs of a fuzzy controller to generate the reference of the battery current. Then such a reference is tracked by a PI regulator. The authors in [18] use two SMCs for the SC and battery currents and a Lyapunov based controller to regulate the DC bus voltage. The paper includes the stability analysis to show the global stability of the system. However, the SMCs proposed in [18, 22] are used to calculate a duty cycle and not to generate the switching signals of the converters; moreover, the design procedure is not provided [22] or not clearly explained [18].

It is important to highlight that any the HESS systems described before guarantee that the battery currents fulfill the slew-rate limitation provided by the manufacturer when there are fast perturbations in the DC bus. Therefore, the battery may be submitted to a high slew-rate current, which reduces its lifetime.

This paper proposes a charger/discharger system for a HESS using a series architecture. The battery is connected to an auxiliary capacitor (not necessarily a SC) through a buck/boost converter. In turn, the auxiliary capacitor is connected to the DC bus by another buck/boost converter. The control system if formed by two cascade controllers, where the inner loops are SMCs of the converters' inductors currents and the outer loops are linear controller to limit the battery current slew-rate, with one converter, and regulate the DC bus voltage, with the other converter. The paper provides the controllers' design procedure and their validation with simulation results. The proposed HESS is able to regulate the voltage of a DC bus when the battery is within its

maximum and minimum state-of-charge, while keeping the battery current slew-rate below its maximum value. Moreover, buck/boost converters improves the flexibility of the system, since it facilitates the connection of batteries, auxiliary capacitors, and DC buses with different voltages.

2. Power circuit

Figure 1 presents the proposed double-stage battery power system aimed at improving both the battery operation conditions and the voltage quality of the load.

The first stage is a bidirectional buck/boost converter designed and regulated to limit the slew-rate of the battery current to a safe value. Such a first stage has a highfrequency capacitor C_{HF} connected in parallel with the battery, which is in charge of absorbing the switching ripple of the current generated by the buck/boost converter.

However, the mean current value requested to the batterycould exhibit high frequency transients, e.g. step current transients; therefore, this stage must be controlled to ensure that the mean battery current fulfills the slew-rate restriction required for a safe operation. The buck/boost converter is formed by two Mosfets, M_{1b} and M_{2b}, and by an inductor L_b. Moreover, this stage provides or extracts current to an auxiliary capacitor C_a, which enables to isolate the battery from the load current i_{dc}.

This stage is controlled with a cascade structure: an inner controller regulates the inductor current, while an outer controller limits the slew-rate of the battery current and ensures a power balance into the auxiliary capacitor. The current controller produces the control signals of the Mosfets, u_b for M_{1b} and $\bar{u}= 1-u_b$ for M_{2b}, while the outer controller produces the current reference i_{Rb} for the current controller.

The second stage is also a bidirectional buck/boost converter, which is designed and regulated to provide a stable voltage to the load. This buck/boost converter is formed by two Mosfets, M_{1c} and M_{2c}, and by an inductor L_c. This stage provides or extracts current from the auxiliary capacitor C_a to be delivered to the output capacitor C_{dc}. Moreover, this stage must compensate the perturbations of the load current i_{dc}, hence behaving as an ideal voltage source.

The control of this stage is also based on a cascade structure: an inner controller regulates the inductor current, while an outer controller regulates the load voltage depending on some performance criterion, e.g. maximum voltage deviation.

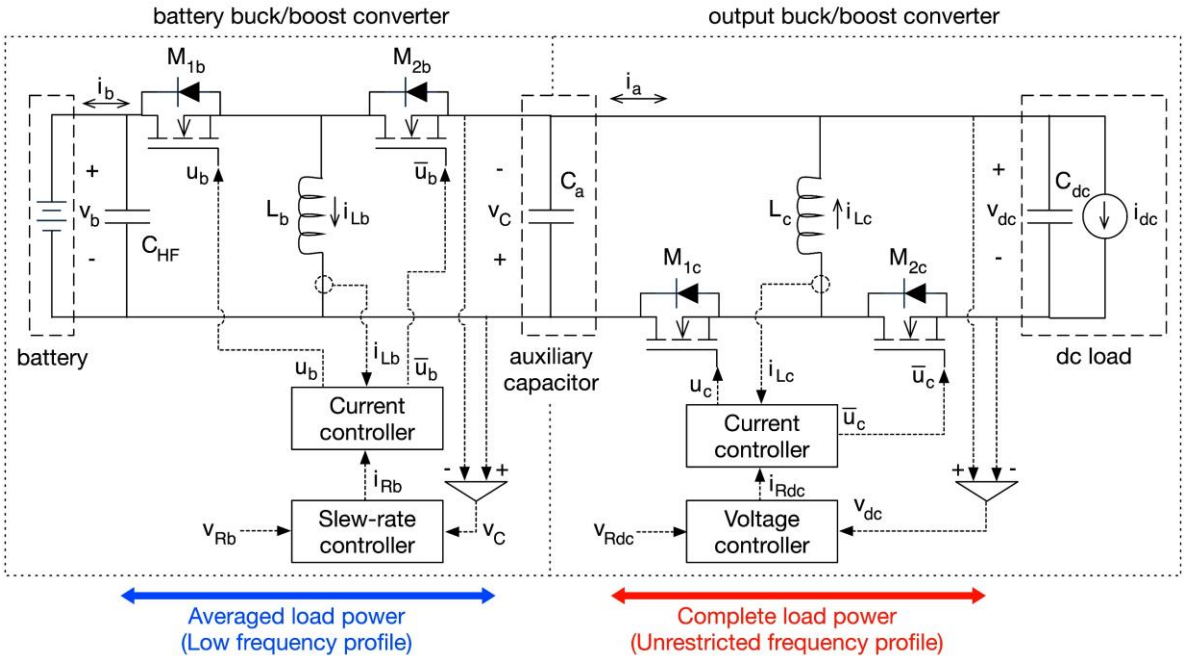

Figure 1. Double-stage battery power system

The current controller produces the control signals of the Mosfets, u_c for M_{1c} and $\bar{u}_c = 1 - u$ for M_{2c}, while the outer controller produces the current reference i_{Rdc} for the current controller. Finally, the load is modeled with the capacitor C_{dc} in parallel with the current source i_{dc}. Such a circuit is able to reproduce the behavior of any load by correctly defining the current profile of i_{dc}.

Figure 1 also shows the difference of the power flows imposed by the controllers: the second stage provides the complete load power, hence no frequency restriction is imposed to the load current; instead, the first stage only provides the averaged load power, hence only low frequency current components are allowed. However, the outer controller of the first stage will charge, respecting the current slew-rate (slowly), the auxiliary capacitor over time. Therefore, the current requested by the load is provided protecting the battery from high-frequency transients. Moreover, it must be pointed out that this solution adopts the same number and type of converters reported in other solutions such as [8, 10, 12, 18, 26, 27, 28, 29, 30, 31, 32]; hence no additional costs are introduced due to the power stages. Similarly, the controllers have the same nature that the solutions reported in [8, 15, 18]; hence no additional costs are introduced due to the control stages. The following section presents the mathematical model of the buck/boost stages and describes the design of the inner current controller.

3. Stage model and current controller

Taking into account that both stages of the power circuit in Fig. 1 are based on bidirectional buck/boost structures, this section presents a general model of a single buck/boost stage. Such a model is used to design the current controller for the single stage, which is the same for both stages of the complete power circuit.

Figure 2 presents the circuital model of a single buck/boost stage, where the input voltage source is v_i, the Mosfets are M_1 and M_2, the inductor is L, the control signals are u and $\bar{u} = 1 - u$, the output capacitor is C and the output voltage is v_o. For this general circuit, the reference of the current controller is i_R, and the reference of the outer controller is v_R. Table 1 presents the correspondence of the parameters and variables of the single stage model with the first and second stages parameters and variables. The C_{HF} capacitor is not considered in the dynamic analysis since it is connected in parallel with the battery, hence its voltage is imposed by the battery and it does not introduce a new state variable.

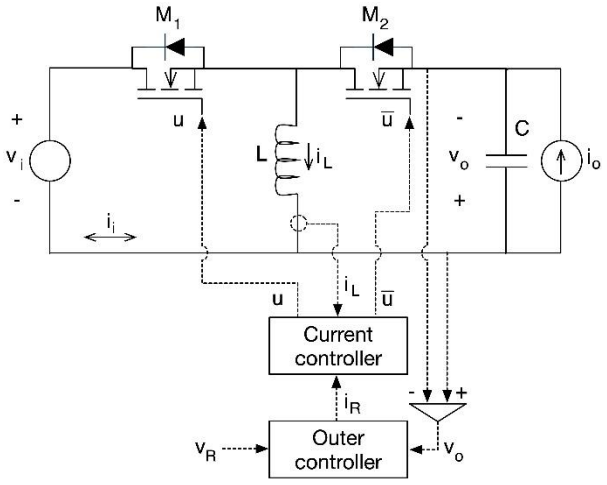

Figure 2. Circuital model of a single buck/boost stage.

Table 1. Parameters and variables correspondence

Single stage model	First stage	Second stage
L, C	L_b, C_a	L_c, C_{dc}
M_1, M_2	M_{1b}, M_{2b}	M_{1c}, M_{2c}
v_i, v_o, i_L	v_b, v_C, i_{Lb},	v_c, v_{dc}, i_{Lc},
u,$\bar{u}$	u_b, $\bar{u}_b$,	u_c, $\bar{u}_c$,
v_R , i_R	v_{Rb}, i_{Rb}	v_{Rdc}, i_{Rdc}

Expressions (1) and (2) report the switched differential equations that describe the behavior of both the inductor current i_L and output voltage v_o of the buck/boost stage.

$$L.\frac{di_L}{dt} = v_i.u - v_o.\bar{u} \quad (1)$$

$$C.\frac{dv_o}{dt} = i_L.\bar{u} - i_o \quad (2)$$

To regulate the inductor current of the stage, a sliding mode controller (SMC) is proposed, which provides robustness to changes on both the parameters and the operation conditions [33]. Moreover, a well designed SMC ensures global stability, which is needed in this application due to the wide range of operation conditions: charging the source (negative inductor current), discharging the source (positive inductor current), stand-by mode (null inductor current), boosting voltage, reducing voltage or ensuring the same voltage at both the input and output ports. To fulfill those conditions, this paper proposed to design the SMC using the following switching function F and sliding-surface S_F:

$$F = i_L - i_R \quad S_F = \{F = 0\} \quad (3)$$

To ensure the global stability of the SMC three conditions must be fulfilled [34]: transversality,

reachability and equivalent control. Those conditions are analyzed in the following subsections.

3.1. Modelo de un Supercondensador utilizando la DFC

The transversality condition verifies the control signal u is present into the switching function derivative $\frac{dF}{dt}$. This is a necessary condition for controllability, otherwise the controller will not be able to modify the trajectory of the system. The mathematical formalization of this condition is given in (4).

$$\frac{d}{du}\left(\frac{dF}{dt}\right) \neq 0 \tag{4}$$

The first step to evaluate the transversely condition is to calculate, explicitly, the switching function derivative:

$$\frac{dF}{dt} = \frac{di_L}{dt} - \frac{di_R}{dt} \tag{5}$$

$$\frac{dF}{dt} = \frac{v_i.u - v_o.\bar{u}}{L} - \frac{di_R}{dt} \tag{6}$$

Replacing expression (6) into (4) leads to inequality (7), which is always positive since L, v_i and v_o are positive quantities.

$$\frac{d}{du}\left(\frac{dF}{dt}\right) = \frac{v_i + v_o}{L} > 0 \tag{7}$$

Therefore, expression (7) verifies that the proposed SMC always fulfills the transversality condition.

3.2. Reachability conditions

The reachability conditions verifies that the system, under the action of the SMC, is able to reach the surface $S_F = \{F = 0\}$. In practical terms, those conditions verify that the switching function derivative is positive $\left(\frac{dF}{dt} > 0\right)$ when the switching function is operating under the surface ($F < 0$); similarly, the switching function derivative must be negative $\left(\frac{dF}{dt} < 0\right)$ when the switching function is operating above the surface ($F > 0$).

The formalization of the reachability conditions depends on the sign of the transversality value: a positive transversality value, as the one given in (7), implies that a positive change on u (from 0 to 1) produces a positive switching function derivative $\left(\frac{dF}{dt} > 0\right)$, and a negative change on u (from 1 to 0) produces a negative switching function derivative $\left(\frac{dF}{dt} < 0\right)$. In conclusion, the formalization of the reachability conditions is given in (8).

$$\lim_{F\to 0^-} \frac{dF}{dt}\bigg|_{u=1} > 0 \ \wedge \ \lim_{F\to 0^+} \frac{dF}{dt}\bigg|_{u=0} < 0 \tag{8}$$

Replacing the switching function derivative (6) into (8) leads to restriction (9), which defines the minimum and maximum derivatives of the current reference ensuring the reachability conditions. It must be noted that those limits are the minimum and maximum derivatives of the inductor current, which are calculated from (1) with u = 0 and u = 1, respectively.

$$-\frac{v_o}{L} < \frac{di_R}{dt} < \frac{v_i}{L} \tag{9}$$

Therefore, the previous equation ensures that the proposed SMC can reach the sliding surface, and also it demonstrates that the SMC provides the maximum speed achievable with the converter.

3.3. Equivalent control condition

The equivalent control evaluates the local stability by analyzing the duty cycle saturation. This is performed by calculating the averaged value ueq of the control signal u, which is equal to the duty cycle d: $u_{eq} = \frac{1}{T}.\int_0^{T_{sw}} u\, dt = d$ where T_{sw} is the switching period. The equivalent control must be analyzed when the system is operating into the surface $F = 0$ with a parallel trajectory, i.e. $\frac{dF}{dt} = 0$ [33].

Then, replacing (6) into $\frac{dF}{dt} = 0$ leads to the following expression for u_{eq}:

$$u_{eq} = \frac{v_o + L.\frac{di_R}{dt}}{v_i + v_o} = d \tag{10}$$

The classical equivalent control condition is evaluated as $0 < u_{eq} < 1$, which evaluates that the duty cycle is not saturated, i.e. $0 < d < 1$. This is a necessary condition for both controllability and local stability. Finally, replacing equation (10) into $0 < u_{eq} < 1$ results in the same limits for $\frac{di_R}{dt}$ given in (9). This is expected since Sira-Ramirez demonstrated in [34] a dc/dc converter under the action of a SMC that fulfills both transversality and reachability conditions also fulfills the equivalent control condition. In conclusion, the proposed SMC based in (3) is globally stable, hence it guarantees that $i_L = i_R$.

4. Outer controllers

There are two outer controllers to be designed: the battery slew-rate controller and the output voltage controller. Those outer controllers are designed considering the equivalent dynamics of the SMC, i.e. $i_L = i_R$. Moreover, since the control signals of the Mosfets are defined by the SMC, then the equivalent dynamics are analyzed by averaging the state-variables into the switching period, i.e. $u_{eq} = d$. Therefore, by replacing i_L by i_R and u by d into equation (2) leads to the equivalent dynamics of the capacitor voltage given in (11), where the duty cycle d is the steady-state value given in (12).

$$\frac{dv_o}{dt} = \frac{i_R.(1-d) - i_o}{C} \tag{11}$$

$$d = \frac{v_o}{v_o + v_i} \tag{12}$$

Such an equivalent voltage dynamics, represented in the Laplace domain, is given in (13), where V_o, I_R and I_o are the Laplace representations of v_o, i_R and i_o, respectively.

$$V_o = \frac{I_R.(1-d) - I_o}{S \cdot C} \tag{13}$$

The outer controller, whose transfer function is named G_{oc}, defines the current controller reference I_R as follows: $I_R = G_{oc} \cdot (V_R - V_o)$. However, taking into account that the voltage reference v_R of the circuital model in Fig. 2 is a constant value (hence also V_R is constant), the smallsignal closed-loop dynamics (including the outer controller) of both V_o and I_R depend only on I_o, i.e. the current perturbations imposed by the load, as follow:

$$V_o = \frac{-1}{C \cdot s + (1-d) \cdot G_{oc}} \cdot I_o \tag{14}$$

$$V_o = \frac{G_{oc}}{C \cdot S + (1-d) \cdot G_{oc}} \cdot I_o \tag{15}$$

The following subsections describes the design of the outer controllers for both stages.

4.1. First stage: slew-rate controller

For this stage, the adopted controller is a constant gain α (i.e. $G_{oc} = \alpha$), which leads to the closed-loop dynamics of V_o and I_R reported in (16) and (17), respectively.

$$V_o = \frac{-1}{C \cdot s + (1-d) \cdot \alpha} \cdot I_o \tag{16}$$

$$I_R = \frac{\alpha}{C \cdot s + (1-d) \cdot \alpha} \cdot I_o \tag{17}$$

Taking into account that the main objective of this controller is to limit the slew-rate of the battery current, the design of α is performed using equation (17). The design considers the worst-case scenario for a load perturbation, i.e. the fastest transients possible, which corresponds to a step current with amplitude $|Io|$ (i.e. $I_o = |I_o| /s$). Replacing the $I_o = |I_o| /s$ into equation (17), and applying the inverse Laplace transformation, the time-domain waveform of the current reference given in (18) is obtained.

$$i_R = \frac{|I_O|}{1-d} \cdot \left[1 - e^{-\frac{\alpha \cdot (1-d) \cdot t}{C}}\right] \tag{18}$$

The derivative of the current reference is reported in (19), which must be limited to constrain the slew-rate of the battery current. Since the exponential term of (19) decreases with increments in t, the maximum value of (19) occurs at $t = 0$ as it is reported in (20).

$$\frac{di_R}{dt} = \frac{|I_O|}{C} \cdot \left[e^{-\frac{\alpha \cdot (1-d) \cdot t}{C}}\right] \tag{19}$$

$$máx = \left(\frac{di_R}{dt}\right) = \frac{|I_O| \cdot \alpha}{C} \tag{20}$$

The battery current is obtained from Fig. 2 as $i_i = d \cdot i_L$. Since under the action of the SMC $i_L = i_R$, hence dii dt = $d \cdot \frac{di_R}{dt}$. To respect the safe slew-rate S_R of the battery current, the following expression must be fulfilled:

$$máx = \left(\frac{di_R}{dt}\right) = d \cdot máx = \left(\frac{di_R}{dt}\right) \leq S_R \tag{21}$$

Replacing expression (20) into (21) leads to the design expression for a:

$$\alpha \leq \frac{C \cdot S_R}{d \cdot |I_O|} \tag{22}$$

Finally, from the steady-state error in the output voltage of this first stage, which corresponds to the voltage of the auxiliary capacitor, is calculated from (16) as:

$$\Delta V_\alpha = -\frac{|I_O|}{\alpha \cdot (1-d)} \tag{23}$$

Such a voltage deviation does not introduce problems in terms of the load voltage regulation since the second stage is also a buck/boost topology. Moreover, the

auxiliary capacitor C_a could be designed to limit that voltage deviation into a desired range.

4.2. Second stage: voltage controller

For this stage, the adopted controller is a gain, a zero and a pole as given in (24), which leads to the closed-loop dynamics of V_o reported in (25).

$$G_{oC} = \alpha \cdot \frac{s + \mathrm{b}}{s} \tag{24}$$

$$\frac{V_o}{} = \frac{-s}{C \cdot s^2 + (1 - d) \cdot \alpha \cdot s + (1 - d) \cdot \alpha \cdot b} \cdot I_o \tag{25}$$

Since the output (load) voltage dynamic has a second order transfer function, this solution adopts a damping ratio equal to one (ρ = 1), which leads to the following transfer function:

$$V_o = \frac{-s}{C \cdot (s + 2 \cdot b)^2} \cdot I_o \; with \; b = \frac{(1 - d) \cdot \alpha}{4 \cdot C} \tag{26}$$

For the worst-case scenario for a load perturbation, defined as $I_o = |I_o| / s$, the time-domain waveform of the load voltage (27) is defined as follows:

$$v_o = -\frac{|I_O|}{C} \cdot t \cdot e^{-2 \cdot b \cdot t} \tag{27}$$

This controller is designed to ensure a safe maximum load voltage deviation ΔV_{dc}. The calculation of such a quantity requires to calculate the time derivative of v_o as follows:

$$\frac{dv_o}{dt} = -\frac{|I_O|}{C} \cdot (2 \cdot b \cdot t - 1) \cdot e^{-2 \cdot b \cdot t} \tag{28}$$

Solving equation (28), and replacing such a time value into (27), leads to the maximum deviation ΔV_{dc} reported in (29), which is used to calculate b for a desired ΔV_{dc}. Then, equation (26) is used to calculate a for that particular b value.

$$\Delta V_{dc} = -\frac{|I_O| \cdot e^{-1}}{2 \cdot C \cdot b} \tag{29}$$

Finally, since b in (26) depends on the duty cycle, the calculations must be done for the worst-case scenario, i.e. lowest input voltage v_i, which for this second stage corresponds to the lowest auxiliary capacitor voltage.

4.3. Controller implementation

The classical hysteresis comparator is adopted [33] to implement the SMC. Such a technique introduces a hysteresis band H around the sliding-surface to limit the switching frequency, which transforms the sliding surface (3) to the practical expression given in (30). Basedon that practical sliding-surface, and on the reachability, conditions given in (8), the control laws for the SMC of both the first and second stages are reported in (31) and (32), respectively.

$$|i_L - i_R| < \frac{H}{2} \tag{30}$$

$$u_b = \begin{cases} 0 \;\; if \;\; i_{Lb} - i_{Rb} > \dfrac{H}{2} \\ 1 \;\; if \;\; i_{Lb} - i_{Rb} < -\dfrac{H}{2} \end{cases} \tag{31}$$

$$u_C = \begin{cases} 0 \;\; if \;\; i_{Lc} - i_{Rdc} > \dfrac{H}{2} \\ 1 \;\; if \;\; i_{Lc} - i_{Rdc} < -\dfrac{H}{2} \end{cases} \tag{32}$$

5. Result

The validation of the design procedure considers the following parameters, but any other values can be adopted: $L_b = L_c = 100 \; \mu H$, $C_{HF} = C_a = C_{dc} = 100 \; \mu F$, $v_b = v_C = v_{dc} = 12 \; V$, therefore $v_{Rb} = v_{Rdc} = 12 \; V$. The performance criteria are: $\Delta V_{dc} = 0{,}5 \; V$ for load current transients with amplitude $|I_o| = 1 \; A$, and a maximum slew-rate of the battery current $S_R = 4 \; A/ms$.

Applying the design procedure reported in the previous sections, the parameter a = 0,8 for the slew-rate controller of the first stage was calculated. Similarly, the parameters for the load voltage controller of the second stage are b = 3,6788 × 10^3 and a = 3,5490. Figure 3 presents the simulation of expressions (18) and (19) considering the designed a parameter and a step-current perturbation in the load with amplitude $|I_o| = 1 \; A$: this simulation confirms that the reference signals fulfill the slew-rate limitations. Such a condition is explicit in the waveforms at the middle of the figure, where the derivatives of both references are under the design limit $\left(\frac{S_R}{d} = 8 \; A/ms\right)$. Finally, the waveforms at the bottom of the figure confirms that the battery current slew-rate is always under the safe limit $S_R = 4 \; A/ms$, hence fulfilling the first design criterion.

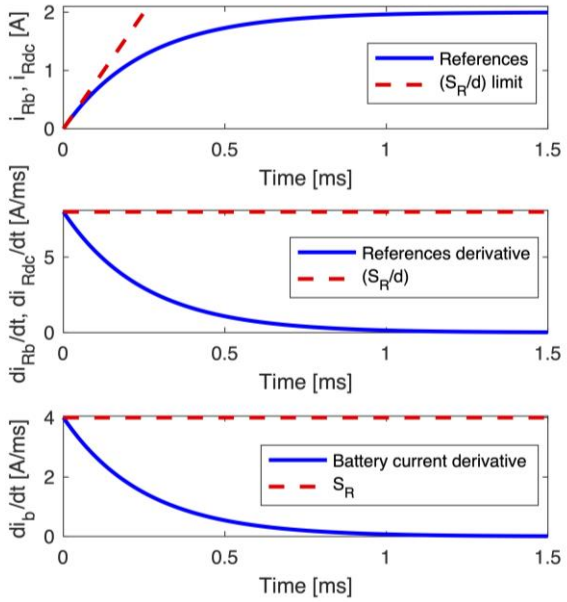

Figure 3. Slew-rate limitation of the reference currents and battery current

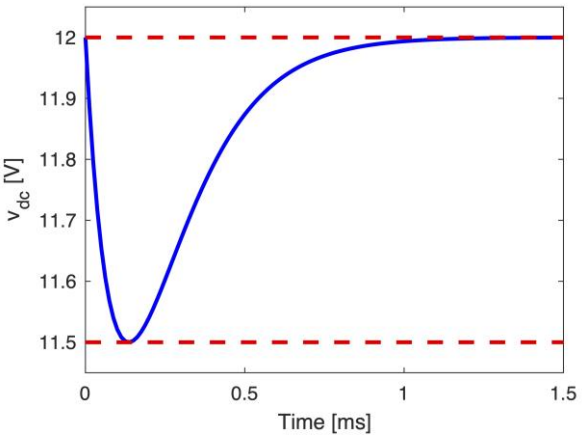

Figure 4. Load voltage regulation

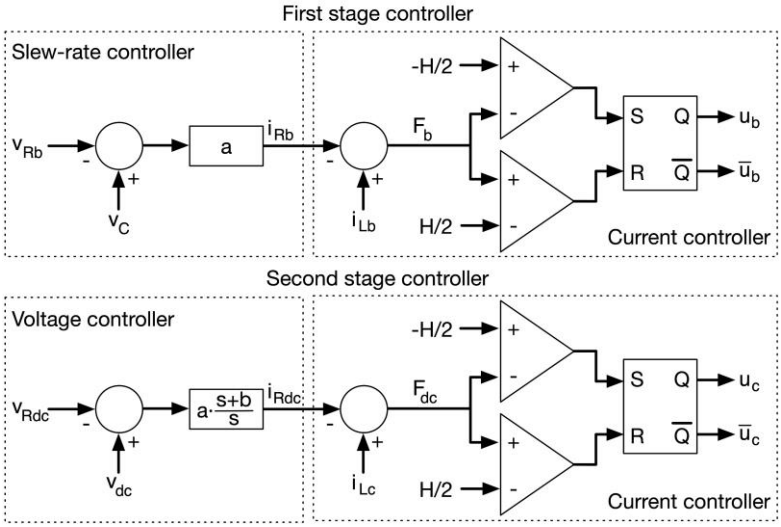

Figure 5. Implementation of the power circuit controllers

Figure 4 presents the simulation of expression (27) considering the designed *a* and *b* parameters for the same stepcurrent perturbation in the load: the simulation confirms that the proposed controller constraints the voltage deviation to the designed limit ΔV_{dc} = 0,5 *V*, hence fulfilling the second design criterion. Figure 5 present the circuits for both controllers, where the SMC control laws are implemented using S-R Flip-Flops, classical comparators and adders; while the slew-rate and voltage controllers are implemented using linear functions. Then, the complete power circuit of Fig. 1 and the controllers circuits of Fig. 5 were implemented in the power electronics simulator PSIM adopting H = 0,3 *A* to limit the switching frequency up to 300 kHz.

Figure 6 presents the circuital simulation of the complete battery power system performed in PSIM. The simulation considers the battery in the three possible operation conditions: discharge (positive current), charge (negative

current) and stand-by (null current). The simulation verifies the correct regulation of the load voltage by fulfilling the maximum deviation limit ΔV_{dc} = 0,5 *V*, hence confirming the simulation of Fig. 4. The figure also presents the auxiliary capacitor voltage, where it is observed the support provided by this capacitor, which enables the power circuit to regulate the slew-rate of the battery current. Figure 6 also presents battery current, which fulfills the dynamic restriction of the maximum slew-rate S_R; such a restriction is also evident in the maximum slew-rate of i_{Lb}, hence confirming the simulation of Fig. 3. The switching functions of both SMC are also reported in Fig. 6, which shows that both converters always operate inside the hysteresis bands: such a behavior verifies the global stability of the SMCs, hence the safe operation of both the battery and the load is guaranteed.

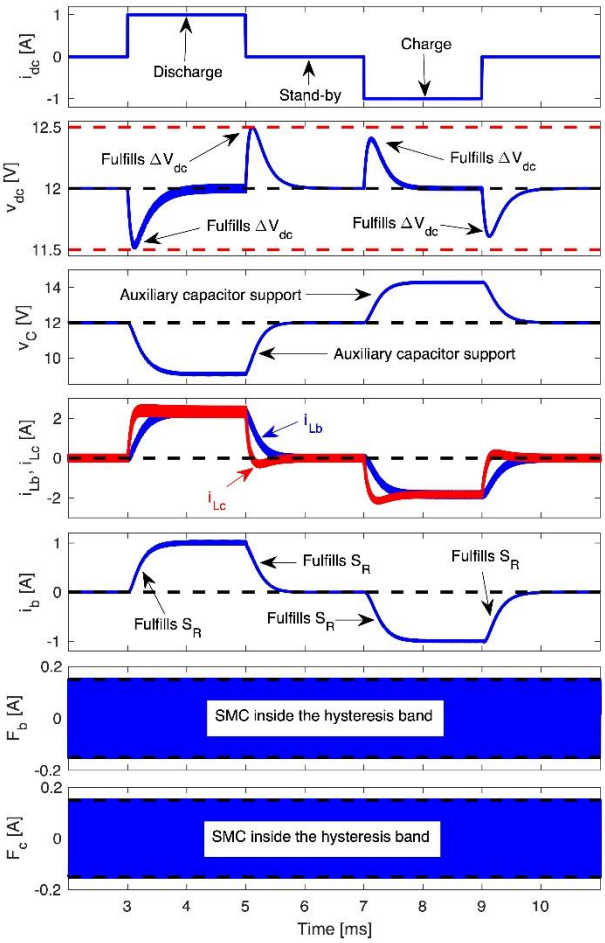

Figure 6. Circuital simulation performed in PSIM

The global stability of the proposed solution, demonstrated by both the analytical and simulation results, significantly improves the reliability and safety of the hybrid power system in comparison with other solutions based on linear controllers, such as the ones reported in [10, 13, 17, 29, 35, 36]. Moreover, the limitation of the current slope, provided by proposed solution, also reduced the battery degradation in comparison with solutions where such a limitation is not considered, e.g. [8, 10, 13, 15, 17, 18, 30, 31].

In any case, with the aim of illustrating the improvement provided by the proposed solution, Fig. 7 presents a comparison of the performance of both the proposed and a classical solution. To provide a fair comparison, the classical solution also considers SMC for the current controllers, but such a classical solution does not consider limitation on the current derivative of the battery, which is the case found in literature. The simulation considers a fast current transient in the load current (steplike change), and both the proposed and classical solutions provide a satisfactory regulation of the bus voltage. However, since the classical solution does not include a limitation on the battery current derivative, the slew-rate of the battery current is much higher than the safe limit S_R. Instead, the proposed solution fulfills such a limitation, hence protecting the battery. In conclusion, despite both solutions provide an accurate bus voltage regulation, only the proposed solution protects the battery from high-frequency current transients since such a derivative limitation is considered into the SMC design.

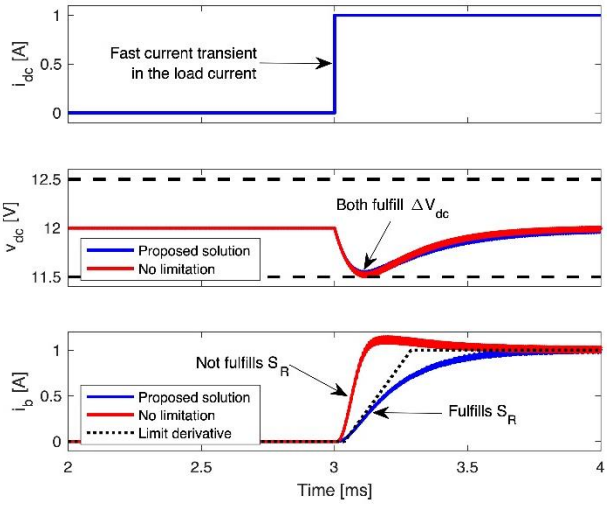

Figure 7. Comparison of both the proposed and classical solutions

6. Conclusions

A HESS with a series architecture formed by a battery, an auxiliary capacitor (not necessarily a SC), two

buck/boost converters and a control system has been introduced. The control system is formed by two cascaded controllers, one for the converter connecting the battery with the auxiliary capacitor, and the other for the convert interfacing the auxiliary capacitor with the DC bus. The inner loops of both controllers are SMCs of the inductors' current, while the outer loop of the battery converter is a P controller that limits the current slew-rate, and the outer loop of the auxiliary capacitor converter is a PI controller to regulate the DC bus voltage. A detailed design procedure has been introduced, and the validation with simulation results has been performed. Those results show that the proposed system fulfills the control design requirements regarding slew-rate limitation, DC bus voltage regulation, and current tracking for both the battery and the auxiliary capacitor. Moreover, the buck/boost converters provide additional flexibility to connect batteries and auxiliary capacitors with voltages lower, equal or higher than the DC bus voltage.

References

[1] International Energy Agency (IEA), "Energy Storage - Tracking Clean Energy Progress," pp. 1–6, 2019.

[2] S. Hajiaghasi, A. Salemnia, M. Hamzeh, "Hybrid energy storage system for microgrids applications: A review," *Journal of Energy Storage*, vol. 21, no. 2018, pp. 543–570, 2019, doi: 10.1016/j.est.2018.12.017

[3] X. Chang, Y. Li, W. Zhang, N. Wang, W. Xue, "Active Disturbance Rejection Control for a Flywheel Energy Storage System," *IEEE Transactions on Power Electronics*, vol. 62, no. 2, pp. 991– 1001, 2015.

[4] C. A. Ramos-Paja, J. D. Bastidas-Rodríguez, D. González, S. Acevedo, J. Peláez-Restrepo, "Design and Control of a Buck/A ¸SBoost Charger-Discharger for DC-Bus Regulation in Microgrids," *Energies*, vol. 10, no. 11, pp. 1–26, 2017.

[5] W. Jing, C. H. Lai, W. S. Wong, M. L. Wong, "Dynamic power allocation of battery-supercapacitor hybrid energy storage for standalone PV microgrid applications," *Sustainable Energy Technologies and Assessments*, vol. 22, pp. 55–64, 2017, doi: 10.1016/j.seta.2017.07.001

[6] R. Georgious, J. Garcia, P. Garcia, and M. Sumner, "Analysis of hybrid energy storage systems with DC link fault ride-through capability," in *ECCE 2016 - IEEE Energy Conversion Congress and Exposition, Proceedings*, 2016, pp. 1–8.

[7] R. Sedaghati, M. R. Shakarami, "A novel control strategy and power management of hybrid PV/FC/SC/battery renewable power system-based grid-connected microgrid," *Sustainable Cities and Society*, vol. 44, pp. 830–843, 2019, doi: 10.1016/j.scs.2018.11.014

[8] A. Etxeberria, I. Vechiu, H. Camblong, J. M. Vinassa, "Comparison of sliding mode and PI control of a hybrid energy storage system in a microgrid application," *Energy Procedia*, vol. 12, pp. 966–974, 2011, doi: 10.1016/j.egypro.2011.10.127

[9] J. Li, R. Xiong, Q. Yang, F. Liang, M. Zhang, W. Yuan, "Design/test of a hybrid energy storage system for primary frequency control using a dynamic droop method in an isolated microgrid power system6," *Applied Energy*, vol. 201, pp. 257– 269, 2017.

[10] A. Narvaez, C. Cortes, C. Trujillo, "Topologies for battery and supercapacitor interconnection in residential microgrids with intermittent generation," *Ingeniería*, vol. 25, no. 1, pp. 1–24, 2020.

[11] H. El Fadil, F. Giri, "Sliding Mode Control of Fuel Cell and Supercapacitor Hybrid Energy Storage System," in *8th Power Plant and Power System Control Symposium - IFAC Proceedings Volumes. IFAC*, 2012, pp. 669 – 674.

[12] B. Yang, J. Wang, X. Zhang, J. Wang, H. Shu, S. Li, T. He, C. Lan, T. Yu, "Applications of battery/supercapacitor hybrid energy storage systems for electric vehicles using perturbation observer based robust control," *Journal of Power Sources*, vol. 448, pp. 227444, 2020, doi: 10.1016/j.jpowsour.2019.227444

[13] O. Veneri, C. Capasso, S. Patalano, "Experimental investigation into the effectiveness of a super-capacitor based hybrid energy storage system for urban commercial vehicles," *Applied Energy*, vol. 227, pp. 312–323, 2018, doi: 10.1016/j.apenergy.2017.08.086

[14] M. Sellali, S. Abdeddaim, A. Betka, A. Djerdir, S. Drid, M. Tiar, "Fuzzy-Super twisting control implementation of battery/super capacitor for electric vehicles," *ISA Transactions*, vol. 95, pp. 243–253, 2019, doi: 10.1016/j.isatra.2019.04.029

[15] B. Wang, J. Xu, D. Xu, Z. Yan, "Implementation of an estimator-based adaptive sliding mode control strategy for a boost converter based battery/supercapacitor hybrid energy storage system in electric vehicles," *Energy Conversion and Management*,

vol. 151, pp. 562–572, 2017, doi: 10.1016/j.enconman.2017.09.007

[16] S. Ahmadi, S. M. Bathaee, A. H. Hosseinpour, "Improving fuel economy and performance of a fuel-cell hybrid electric vehicle (fuel-cell, battery, and ultra-capacitor) using optimized energy management strategy," *Energy Conversion and Management*, vol. 160, pp. 74–84, 2018, doi: 10.1016/j.enconman.2018.01.020

[17] L. Sun, P. Walker, K. Feng, N. Zhang, "Multi-objective component sizing for a battery-supercapacitor power supply considering the use of a power converter," *Energy*, vol. 142, pp. 436–446, 2018, doi: 10.1016/ j.energy.2017.10.051

[18] Z. Song, J. Hou, H. Hofmann, J. Li, M. Ouyang, "Sliding-mode and Lyapunov function-based control for battery/supercapacitor hybrid energy storage system used in electric vehicles," *Energy*, vol. 122, pp. 601–612, 2017, doi:10.1016/j.energy.2017.01.098

[19] A. Gee, R. W. Dunn, "Design and analysis of a slidingmode power electronic controlled battery / supercapacitor hybrid energy storage system for remote wind power applications," in *Proceedings of the Universities Power Engineering Conference*, 2011, pp. 1–6.

[20] Z. Li, S. Ben Elghali, R. Outbib, "Energy management for hybrid energy storage systems: A comparison of current tracking control methods," in *Proceedings IECON 2017 - 43rd Annual Conference of the IEEE Industrial Electronics Society*, 2017, pp. 7128–7133.

[21] I. Shchur, Y. Biletskyi, "Battery Currents Limitation in Passivity Based Controlled Battery/Supercapacitor Hybrid Energy Storage System," in *2018 IEEE 38th International Conference on Electronics and Nanotechnology, ELNANO 2018 - Proceedings. IEEE*, pp. 504–510.

[22] J. Wang, Y. Xu, M. Lv, "Modeling and Simulation Analysis of Hybrid Energy Storage System Based on Wind Power Generation System," in *ICCAIS 2018 - 7th International Conference on Control, Automation and Information Sciences. IEEE*, 2018, pp. 422–427.

[23] L. Fangcheng, L. Jinjun, Z. Bin, Z. Haodong, H. S. Ul, "Energy management of hybrid energy storage system (HESS) based on sliding mode control," in *Conference Proceedings - 2012 IEEE 7th International Power Electronics and Motion Control Conference - ECCE Asia, IPEMC 2012, vol. 1. IEEE*, pp. 406–410.

[24] M. Y. Ayad, M. Becherif, A. Djerdir, A. Miraoui, "Sliding mode control of DC bus voltage of a hybrid sources using fuel cell and supercapacitors for traction system," *in IEEE International Symposium on Industrial Electronics*, 2007, pp. 383–388.

[25] S. Najafi-Shad, S. M. Barakati, A. Yazdani, "An effective hybrid wind-photovoltaic system including battery energy storage with reducing control loops and omitting PV converter," *Journal of Energy Storage*, vol. 27, pp. 101088, 2020, doi: 10.1016/j.est.2019.101088

[26] T. Zimmermann, P. Keil, M. Hofmann, M. F. Horsche, S. Pichlmaier, A. Jossen, "Review of system topologies for hybrid electrical energy storage systems," *Journal of Energy Storage*, vol. 8, pp. 78–90, 2016.

[27] Jian Cao, A. Emadi, "A New Battery/UltraCapacitor Hybrid Energy Storage System for Electric, Hybrid, and Plug-In Hybrid Electric Vehicles," *IEEE Transactions on Power Electronics*, vol. 27, no. 1, pp. 122–132, 2012.

[28] M. Soltani, J. Ronsmans, S. Kakihara, J. Jaguemont, P. Van den Bossche, J. van Mierlo, N. Omar, "Hybrid Battery/LithiumIon Capacitor Energy Storage System for a Pure Electric Bus for an Urban Transportation Application," *Applied Sciences*, vol. 8, no. 7, p. 1176, 2018.

[29] B. Wang, J. Xu, R. J. Wai, B. Cao, "Adaptive Sliding-Mode with Hysteresis Control Strategy for Simple Multimode Hybrid Energy Storage System in Electric Vehicles," *IEEE Transactions on Industrial Electronics*, vol. 64, no. 2, pp. 1404–1414, 2017.

[30] J. Li, A. M. Gee, M. Zhang, W. Yuan, "Analysis of battery lifetime extension in a smes-battery hybrid energy storage system using a novel battery lifetime model," *Energy*, vol. 86, pp. 175 – 185, 2015.

[31] G. Ning, B. Haran, B. N. Popov, "Capacity fade study of lithium-ion batteries cycled at high discharge rates," *Journal of Power Sources*, vol. 117, no. 1, pp. 160 – 169, 2003.

[32] R. Han, M. Tucci, A. Martinelli, J. M. Guerrero, G. FerrariTrecate, "Stability Analysis of Primary Plug-and-Play and Secondary Leader-Based Controllers for DC Microgrid Clusters," *IEEE Transactions on Power Systems*, vol. 34, no. 3, pp. 1780–1800, 2019.

[33] T. Siew-Chong, L. Yuk-Ming, T. Chi-Kong, *Sliding Mode Control of Switching Power Converters: Techniques and Implementation*. Boca Raton, London, New York: CRC Press, 2017.

[34] H. Sira-Ramirez, "Sliding Motions in Bilinear Switched Networks," *IEEE Transactions on Circuits and Systems*, vol. 34, no. 8, pp. 919–933, 1987.

[35] H. Zhou, T. Bhattacharya, D. Tran, T. S. T. Siew, A. M. Khambadkone, "Composite Energy Storage System Involving Battery and Ultracapacitor With Dynamic Energy Management in Microgrid Applications," *IEEE Transactions on Power Electronics*, vol. 26, no. 3, pp. 923–930, 2011.

[36] Ke Jin, Mengxiong Yang, Xinbo Ruan, and Min Xu, "ThreeLevel Bidirectional Converter for Fuel-Cell/Battery Hybrid Power System," *IEEE Transactions on Industrial Electronics*, vol. 57, no. 6, pp. 1976–1986, 2010.